

The mechanics of coating delamination in thermal gradients

A.G. Evans^{a,*}, J.W. Hutchinson^b

^a *Materials Department, UCSB, Santa Barbara, CA 93106, United States*

^b *Division of Engineering and Applied Science, Harvard University, Cambridge, MA 02138, United States*

Received 9 November 2006; accepted in revised form 16 March 2007

Available online 27 March 2007

Abstract

Oxide coatings used for various components in the hot section of aero-turbine engines experience temperature gradients at various stages during their flight cycle. One gradient exists during steady-state, due to the combination of the combustion environment next to the free surface and internal cooling of the underlying superalloy substrate. Other gradients develop during cooling of the surface when engine power is reduced. It will be argued that delaminations, when observed within the oxide layer, can only be explained by the presence of a significant stress gradient in the coating, governed by these thermal circumstances. Two extreme cool-down scenarios are envisaged. In one, the surface is cooled suddenly to a lower temperature, followed by slow uniform cooling. In the other, the entire system reduces its temperature uniformly before the temperature gradient in the TBC is eliminated. Criteria for guarding against delaminations within the oxide layer and along the interface with the substrate are provided and the outcome visualized in the form of delamination maps. A comparison with engine experience provides a preliminary assessment of the relevant thermal scenarios, as well as pathways for continuing research.

© 2007 Elsevier B.V. All rights reserved.

Keywords: Thermal barrier coatings; Delamination; Thermal gradients; Densified layer; Vertical cracks; Cool-down

1. Introduction

Oxide coatings have emerged as vital constituents of hot section components in aero-propulsion systems. These act as both thermal (TBC) and environmental (EBC) barriers. Most coated components are actively-cooled from the back-side, resulting in temperature gradients during operation [1–7]. Moreover, during engine shut down, the coating surface can cool quite rapidly, causing additional gradients. Recent observations made on engine components removed from service [8–10] (Fig. 1) have indicated that, when subjected to thermal scenarios of this type, these coatings are susceptible to delamination. Moreover, for representative operating temperatures, the coatings appear to delaminate primarily (but not exclusively) whenever a dense layer has formed in the outermost region. Such dense layers can be caused either by penetration of calcium–magnesium–aluminosilicate (CMAS) deposits ingested into the engine or by sintering of the outermost extremities of the TBC or both.

The delaminations are apparent in two predominant locations (Fig. 1). (i) Shallow delaminations within the dense layer just beneath the surface. (ii) Deep delaminations beneath the dense layer, just above the substrate (bond coat). Fail-safe schemes that eliminate such delaminations are needed for greater coating reliance. The goal of the present article is to establish the requisite mechanics. Where specific examples are warranted, results are presented for both a *thin* ($H=0.1$ mm) TBC, deposited by electron beam methods on aero-engine airfoils (Fig. 1a) and a *thick* ($H=1$ mm) TBC, deposited by air plasma spray (APS) on aero-engine shrouds (Fig. 1b) [9,10]. The properties used are summarized on Table 1, annotated with the data origins and caveats. When required, emphasis is placed on deep delaminations, which are the most debilitating.

Key insights emerge by performing the analysis using the following conservative thermo-mechanical conditions. (Their appropriateness will be assessed, later, by comparing predictions with engine experience). (a) Coatings experience sufficient creep that the stresses relax at the operating condition: a situation envisaged for conventional yttria-stabilized-zirconia (YSZ) TBCs which creep rapidly at typical operating temperatures ($T>900$ °C) [11,12]. (b) Cooling upon engine

* Corresponding author. Tel.: +1 805 893 7839; fax: +1 805 895 8486.

E-mail address: agevans@enr.ucsb.edu (A.G. Evans).

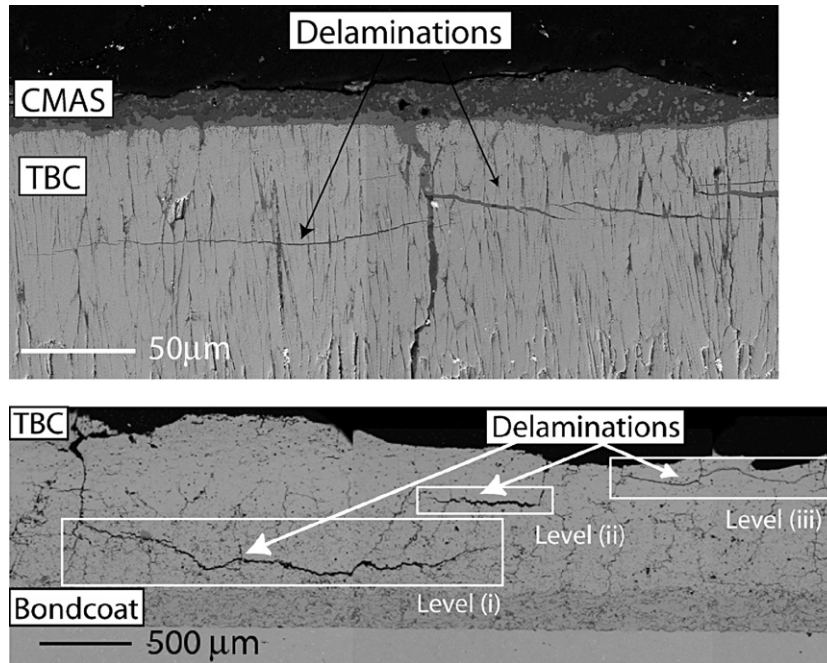


Fig. 1. Examples of delaminations in thermal barrier coatings obtained from components removed from engines subjected to CMAS penetration: (a) Sub-surface mode I delaminations in an airfoil with a TBC made by electron beam physical vapor deposition; the delaminations are within the penetrated zone [9]. (b) Delaminations at several locations within a shroud penetrated by CMAS; the TBC is 1 mm thick and deposited by air plasma spray (APS) [10].

shut down is deemed sufficiently rapid that the material responds thermo-elastically (possible creep relaxation is neglected). (c) Open vertical separations are present that extend from the surface to the substrate. Delaminations, when they occur, invariably originate at such separations [9,10]. These separations either pre-exist after fabrication or develop during high temperature operation (sintering cracks) [13] or form due to tensile stresses induced upon cooling.

Two extreme thermal scenarios are envisaged. (i) As the engine power is reduced, air at (or below) the temperature of the substrate is suddenly imposed on the surface of the coating. This

instantly reduces the surface to the air temperature, followed by uniform cool-down of both the coating and substrate. (ii) The entire system cools uniformly, followed by elimination of the temperature gradient in the TBC. For shallow delaminations, the stress gradients induced during transient cooling are most critical. For deep delaminations, the equilibrium temperatures are most stringent. From a mechanics perspective, the latter are more straightforward and will be analyzed first.

To analyze delaminations parallel to the surface, a crack growth criterion must be specified, as well as various toughness quantities. With reference to Fig. 2, denote the mode I toughness of the dense layer by $\Gamma_{IC}^{(1)}$ and that of the unaffected layer beneath it by $\Gamma_{IC}^{(2)}$, in units of J m^{-2} . Since deep delaminations near or at the interface can extend in mixed

Table 1
The thermomechanical properties for t' -7YSZ TBC coatings used to illustrate the mechanics

	In-plane modulus (GPa)	Thermal expansion coefficient (ppm/°C)	Poisson ratio	Mode I delamination toughness (J m^{-2})	Thermal diffusivity (m^2/s)
As-deposited	20–40	11	0.2	30–45	10^{-7}
CMAS-penetrated	200	11	0.2	30–45	2×10^{-7}

The mode I toughness is from reference [19] for dense t' -7YSZ. There are no reliable data for actual coatings, so a reduction to 30 J m^{-2} has been used to allow for the porosity. The mode II toughness of the coatings has not been measured but results have been reported for predominantly mode II loading. They vary between 100 J m^{-2} [21] and 300 J m^{-2} [22] leading to the choice of mode mixity parameter, $\lambda \geq 0.2$. The modulus values are from reference [23] for the as-deposited TBC. The other properties can be found in various texts such as Wachtman [20]. The modulus of the CMAS-penetrated TBC is taken to be that of the dense YSZ since the fraction of CMAS is small. Likewise the toughness is considered to be unaffected by CMAS penetration.

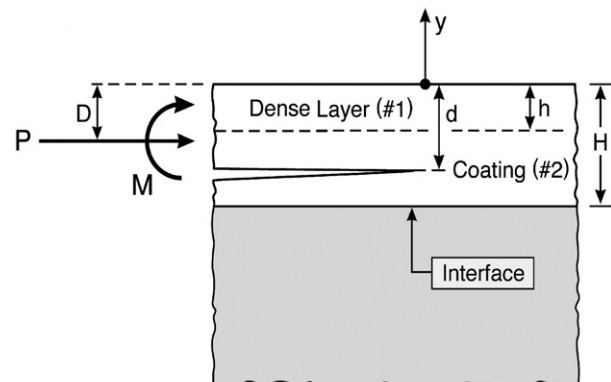


Fig. 2. A schematic of the bilayer coating system identifying the parameters used in the analysis.

mode, a phenomenological expression is used to characterize the toughness dependence on mode mix given by [14]:

$$\Gamma_C^i = \Gamma_{IC}^i [1 + \tan^2((1 - \lambda)\psi)] \quad (1)$$

Here, Γ_{IC}^i is the mode I toughness of the interface and/or the coating just above the interface and the phase angle is given in terms of the stress intensity factors by $\psi = \tan^{-1}(K_{II}/K_I)$. The magnitude of the parameter, λ , sets the mixed mode effect (Fig. 3). For shallow delaminations within the CMAS infiltrated layer, the observations suggest strictly mode I conditions, consistent with the criterion for crack extension in isotropic brittle solids [15], with associated toughness, Γ_{IC}^i . Nevertheless, because of possible toughness anisotropy in the coating, internal delaminations could extend parallel to the surface with some component of mode II. This possibility is retained in the ensuing analysis by using (1) as a general criterion off the interface with appropriate mode I toughness.

The role of the thermally grown oxide (TGO) is implicit in this analysis. As the TGO thickens during high temperature exposure it induces residual stresses in a narrow boundary layer in the superposed TBC [24]. The manifestation of this stress is a reduction in the effective fracture toughness of this region

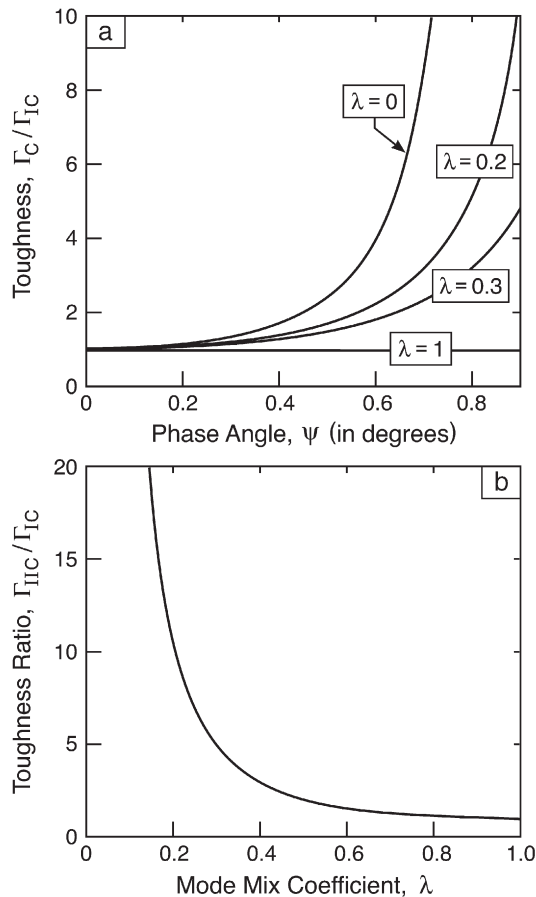


Fig. 3. (a) The trend in mixed mode toughness with phase angle for representative choices of the mode mix coefficient, λ . (b) The ratio of mode II to mode I toughness as a function of λ .

[22,24]. When the magnitude of this reduction is known it can be introduced into the ensuing solutions by adjusting Γ_{IC}^i .

To develop the mechanics systematically, the article is organized in the following manner. (I) The temperatures and stress gradients that develop in the coatings are derived for equilibrium and transient temperature distributions. (II) General results for delamination energy release rates and mode mixity in coatings are presented. (III) Solutions for equilibrium temperatures are derived, with and without a dense outer layer. These are most pertinent to deep delaminations. (IV) The role of the temperature transient is analyzed, with emphasis on shallow delaminations. (V) Results for the energy release rates and mode mix are combined with the fracture criterion to develop delamination maps. (VI) The mechanics predictions are used to derive allowable temperature gradients, which are compared with engine operating scenarios to assess the implications. These solutions are presented for TBCs with and without dense layers.

2. The three layer system

The coating (Fig. 2) has total thickness H and the dense surface layer, if it exists, has thickness h . The delaminations, when they occur are parallel the free surface, at depth d into the coating (Figs. 1 and 2). The substrate is considered to be actively-cooled, giving rise to a temperature drop across the coating while the engine is operating. The initial coating surface temperature is, T_{surface}^i , and interface temperature, $T_{\text{substrate}}^i$. The Young's modulus, Poisson's ratio, thermal conductivity and thermal diffusivity of the coating are denoted by: E_2 , ν_2 , k_2 , κ_2 , respectively. The corresponding quantities for the dense layer are: E_1 , ν_1 , k_1 , κ_1 . The dense layer is considered to have the same coefficient of thermal expansion, taken to be spatially uniform and denoted by α_{coating} , given that porosity has no effect on thermal expansion. [Even with CMAS penetration, α_{coating} is deemed appropriate at the present level of analysis because its volume fraction is quite small [8–10] (<20%) and its thermal expansion unknown]. The thick substrate to which the coating is attached has modulus, $E_{\text{substrate}}$, Poisson's ratio, ($\nu_{\text{substrate}}$), and expansion coefficient, $\alpha_{\text{substrate}}$. The difference in thermal expansion mismatch between the substrate and the coating is denoted by $\Delta\alpha = \alpha_{\text{substrate}} - \alpha_{\text{coating}}$.

3. Temperatures and stress gradients

The objective of this section is to derive temperature distributions and stress gradients for the thermal circumstances envisaged during engine operation and shut down. Initially, the equilibrium temperatures and stresses are ascertained, followed by results for the transient. Solutions are presented for both homogeneous coatings and bilayers with a dense outer layer.

3.1. Equilibrium distributions

Neglecting transient effects associated with thermal diffusivity, continuity of kT_y across the interface between the layers ensures conservation of heat flow. The temperature distribution

within the coating depends on the thermal conductivities as well as the temperatures at the surface and at the substrate, according to

$$T(\eta) = A(\eta)T_{\text{surface}} + B(\eta)T_{\text{substrate}} \quad (2)$$

with

$$\begin{aligned} A(\eta) &= 1 + c_1\eta, & (-h/H < \eta \leq 0) \\ &= c_2(1 + \eta), & (-1 \leq \eta < -h/H) \\ B(\eta) &= -c_1\eta, & (-h/H < \eta \leq 0) \\ &= 1 - c_2(1 + \eta), & (-1 \leq \eta < -h/H) \end{aligned}$$

where $\eta = y/H$, with y defined in Fig. 2. Here,

$$\begin{aligned} c_1 &= \frac{k_2/k_1}{1 - h/H(1 - k_2/k_1)}, \\ c_2 &= \frac{1}{1 - h/H(1 - k_2/k_1)} \end{aligned} \quad (3)$$

Plots of the temperature distribution are given in Fig. 4 for representative values of the material properties.

Denote the initial temperature distribution at the highest heat flux associated with T^i_{surface} and $T^i_{\text{substrate}}$ in (2) by $T^i(\eta)$. At any subsequent stage of cool-down, denote the temperature drop at the surface by, $\Delta T_{\text{surface}} = T^i_{\text{surface}} - T_{\text{surface}}$, and the drop at the substrate by, $\Delta T_{\text{substrate}} = T^i_{\text{substrate}} - T_{\text{substrate}}$. The distribution of the temperature drop, $\Delta T(\eta) = T^i(\eta) - T(\eta)$, which dictates the stresses, is obtained from (2) as:

$$\begin{aligned} \Delta T(\eta) &= (1 + c_1\eta)\Delta T_{\text{sur/sub}} + \Delta T_{\text{substrate}}, & \text{in dense layer} \\ &= c_2(1 + \eta)\Delta T_{\text{sur/sub}} + \Delta T_{\text{substrate}}, & \text{in coating below dense layer} \end{aligned} \quad (4)$$

The temperature quantity, $\Delta T_{\text{sur/sub}} = \Delta T_{\text{surface}} - \Delta T_{\text{substrate}}$ (the instantaneous difference between the temperature drop at the surface and at the substrate) is relevant because the biaxial in-plane stress, $\sigma(\eta)$, is the sum of one contribution proportional to $\alpha_{\text{coating}}\Delta T_{\text{sur/sub}}$ and a second proportional to $\Delta\alpha\Delta T_{\text{substrate}}$.

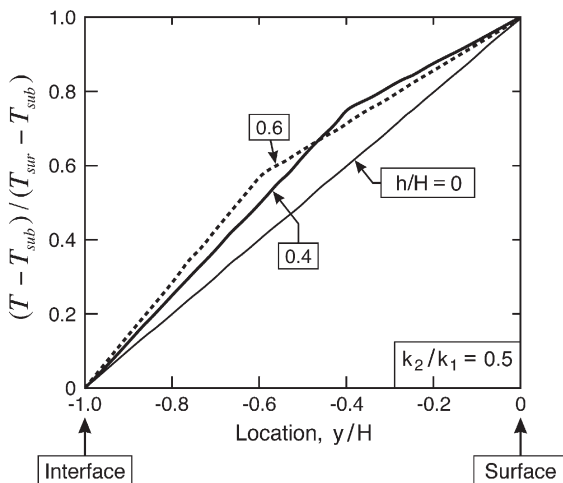


Fig. 4. Equilibrium temperature distributions for two thicknesses of dense layer and for a homogeneous coating ($h/H=0$).

Thus, during cool down, the stress can be written as

$$\begin{aligned} \sigma(\eta) &= \frac{E_1\alpha_{\text{coating}}\Delta T_{\text{sur/sub}}}{(1 - \nu_1)} \{1 + c_1\eta - \Phi\}, & \text{in dense layer} \\ &= \frac{E_2\alpha_{\text{coating}}\Delta T_{\text{sur/sub}}}{(1 - \nu_2)} \{c_2(1 + \eta) - \Phi\}, & \text{in coating below dense layer} \end{aligned} \quad (5)$$

where the dimensionless ratio of mismatch strains is

$$\Phi = \frac{\Delta\alpha\Delta T_{\text{substrate}}}{\alpha_{\text{coating}}\Delta T_{\text{sur/sub}}} \quad (6)$$

The stress gradient, which is proportional to $\alpha_{\text{coating}}\Delta T_{\text{sur/sub}}$ is given by:

$$\begin{aligned} \frac{d\sigma}{dx} &= \frac{E_1\alpha_{\text{coating}}\Delta T_{\text{sur/sub}}}{(1 - \nu_1)H} \frac{k_2/k_1}{1 - (h/H)(1 - k_2/k_1)}, & \text{in dense layer} \\ &= \frac{E_2\alpha_{\text{coating}}\Delta T_{\text{sur/sub}}}{(1 - \nu_2)H} \frac{1}{1 - (h/H)(1 - k_2/k_1)}, & \text{in coating below dense layer} \end{aligned} \quad (7)$$

If the coating surface were suddenly cooled to $T^i_{\text{substrate}}$, the relevant temperature quantity would be, $\Delta T_{\text{sur/sub}} = T^i_{\text{surface}} - (T^i_{\text{substrate}})$, and remain unchanged during subsequent uniform cool-down. The stress gradient would be established by the initial cooling and remain fixed thereafter. However, the absolute stress level changes, becoming less tensile and possibly compressive as the system cools-down. The stress gradient after the system has cooled to ambient is always given by $\Delta T_{\text{sur/sub}} = T^i_{\text{surface}} - T^i_{\text{substrate}}$ in (7), regardless of the cooling history [10].

3.2. Transients

Insightful results are based on those for an infinitely thick homogeneous solid with thermal diffusivity, $\kappa(\text{m}^2 \text{s}^{-1})$, coefficient of thermal expansion, α , Young's modulus, E , and Poisson's ratio, ν . The solid is initially at uniform temperature T^i_{surface} . At $t=0$, the surface is instantaneously cooled from T^i_{surface} to T^f_{surface} , and subsequently held fixed. The transient temperature distribution is the well-known similarity solution

$$T(y, t) = T^i_{\text{surface}} - (T^i_{\text{surface}} - T^f_{\text{surface}}) \text{erfc}(-y/2\sqrt{\kappa t}) \quad (8)$$

where erfc is the complementary error function. The associated biaxial stress acting parallel to the surface is

$$\sigma(y, t) = \frac{E\alpha(T^i_{\text{surface}} - T^f_{\text{surface}})}{(1 - \nu)} \text{erfc}\left(\frac{-y}{2\sqrt{\kappa t}}\right) \quad (9)$$

For a bilayer on a substrate, the corresponding transient temperature distribution, $T(y, t)$, satisfies

$$T_{,yy} = \kappa^{-1}T_{,t} \quad (10)$$

with $\kappa = \kappa_1$, $-h < y \leq 0$ and $\kappa = \kappa_2$, $-H \leq y < -h$. At the interface between these layers, heat flow is conserved according to

$$\lim_{\varepsilon \rightarrow 0} k_1 T_{,y}(-h + \varepsilon, t) = k_2 T_{,y}(-h - \varepsilon, t) \quad (11)$$

The initial temperature distribution, $T(x, 0) = T^i(x)$, is assumed to be in equilibrium, satisfying $T_{,yy} = 0$ for $-H \leq y \leq 0$ together with (11). An exact solution is obtained by making use of an eigenfunction expansion, as detailed in Appendix A. At any instant, denote the equilibrium temperature distribution (2) associated with the current surface and substrate temperatures, $T_{\text{surface}}(t)$ and $T_{\text{substrate}}(t)$, by

$$T_{\text{equil}}(y, t) = A(\eta)T_{\text{surface}}(t) + B(\eta)T_{\text{substrate}}(t)$$

The transient distribution is expressed as

$$T(y, t) = T_{\text{equil}}(\eta, t) + \delta T(\eta, t) \quad (12)$$

The solution for δT , which represents the departure from equilibrium, is given in Appendix A. If the stress vanishes at $T^i(\eta)$, that at any subsequent instant is

$$\begin{aligned} \sigma &= \frac{E_1 [\alpha_{\text{coating}}(T^i(\eta) - T(\eta, t)) - \alpha_{\text{substrate}}(T_{\text{substrate}}^i - T_{\text{substrate}}(t))]}{(1 - \nu_1)}, & -h/H < \eta \leq 0 \\ &= \frac{E_2 [\alpha_{\text{coating}}(T^i(\eta) - T(\eta, t)) - \alpha_{\text{substrate}}(T_{\text{substrate}}^i - T_{\text{substrate}}(t))]}{(1 - \nu_2)}, & -1 \leq \eta < -h/H \end{aligned} \quad (13)$$

Sudden cooling of the surface of the coating is more likely to lead to a non-equilibrium response than temperature changes at the interface due to abrupt changes in gas temperatures impinging upon the surfaces associated with engine burn conditions. In addition, the substantial heat capacity of the superalloy makes rapid temperature changes of the substrate less likely. Thus, emphasis will be on transient effects associated with rapid cooling of the surface as specified by $T_{\text{surface}}(t)$, with the substrate temperature held fixed at $T_{\text{substrate}}^i$. Specifically, cool-down from T_{surface}^i to $T_{\text{surface}}^f \equiv T_{\text{substrate}}^i$ over the period t_{surface}^0 will be investigated with

$$\begin{aligned} T_{\text{surface}}(t) &= T_{\text{surface}}^i + (T_{\text{surface}}^f - T_{\text{surface}}^i)t/t_{\text{surface}}^0, & 0 \leq t \leq t_{\text{surface}}^0 \\ &= T_{\text{surface}}^i, & t > t_{\text{surface}}^0 \end{aligned} \quad (14)$$

while at all times in the substrate,

$$T_{\text{substrate}}(t) = T_{\text{substrate}}^i \equiv T_{\text{surface}}^f \quad (15)$$

The role of the surface cool-down time, t_{surface}^0 , is illustrated by the plots in Fig. 5. If $t_{\text{surface}}^0 \kappa/H^2 \approx 0.5$ or larger, the temperature distribution is nearly in equilibrium. However, if $t_{\text{surface}}^0 \kappa/H^2 \ll 1$, marked departures from equilibrium occur with a large temperature gradient near the surface and associated large stress gradient, with potential for producing shallow delaminations, as will be discussed in the sequel. It should also be noted that when the cool-down is

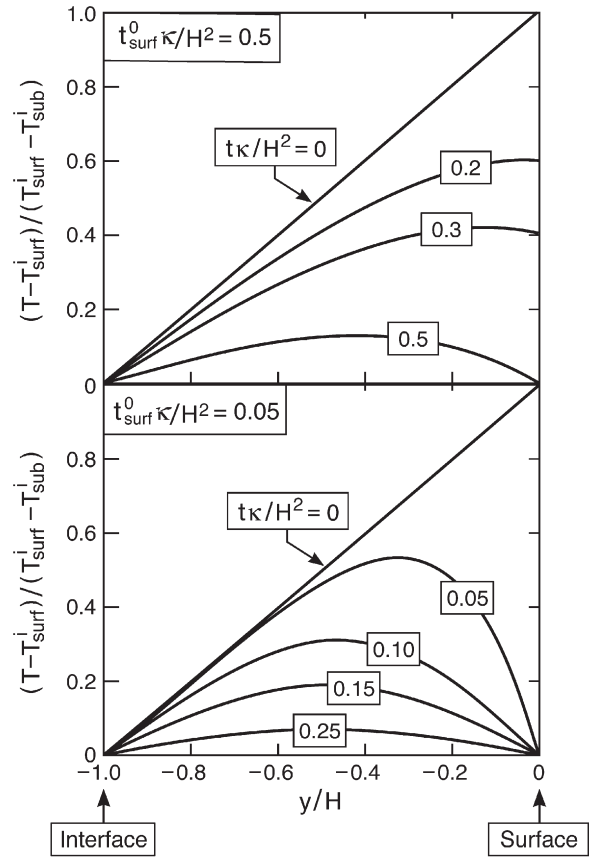


Fig. 5. (a) Transient temperature distributions for a relatively slow surface cool-down period ($t_{\text{surface}}^0 \kappa/H^2 = 0.5$) such that departures from linear equilibrium distributions are small. (b) Transient temperature distributions for a fast surface cool-down period ($t_{\text{surface}}^0 \kappa/H^2 = 0.05$) with large departures from equilibrium.

rapid, as in Fig. 5b with $t_{\text{surface}}^0 \kappa/H^2 = 0.05$, the time required for the coating to equilibrate is $t\kappa/H^2 \approx 0.5$.

4. Stress intensity factors and energy release rates

Basic solutions are presented for delamination stress intensity factors and energy release rates in coatings that experience a stress gradient. One set of results is for delaminations in a homogeneous coating. The other set is for delaminations in a bilayer. The results become the basis for ensuing analyses applicable to the temperature situations described in the preceding section. When the delamination length exceeds the thickness of the coating, the energy release rates are essentially steady-state and determined exactly. The corresponding mode mix is approximate because general results for three-layer systems are non-existent. With y as the coordinate in Fig. 2, let $\sigma(y)$ be the distribution of in-plane stress in the uncracked coating. Define a force/length and moment/length associated with the stress above the delamination plane as:

$$\begin{aligned} P &= \int_{-d}^0 \sigma(y) dy \\ M &= \int_{-d}^0 \sigma(y)(D + y) dy \end{aligned} \quad (16)$$

with D the location of the neutral bending axis above the delamination plane. The basic results for a delamination located

at d below the surface in an infinitely deep, homogeneous layer are:

$$K_I = \frac{1}{\sqrt{2}} \left[Pd^{-1/2} \cos \omega + 2\sqrt{3}Md^{-3/2} \sin \omega \right] \quad (17)$$

$$K_{II} = \frac{1}{\sqrt{2}} \left[Pd^{-1/2} \sin \omega - 2\sqrt{3}Md^{-3/2} \cos \omega \right]$$

$$G = \frac{1}{E} (K_I^2 + K_{II}^2) = \frac{1}{2E} \left(\frac{P^2}{d} + 12 \frac{M^2}{d^3} \right)$$

where the bar indicates the plane strain modulus, $\bar{E} = E/(1-\nu^2)$, and $\omega = 52.1^\circ$ [14]. This result will be applied to the coating with $\bar{E} \equiv \bar{E}_2$, and to a delamination within the dense layer ($0 < d < h$) with $\bar{E} \equiv \bar{E}_1$. Note that, if (17) predicts $K_I < 0$, the crack is closed and pure mode II. However, in all applications envisaged in the present assessment, $M \geq 0$, such that the normal stress between the faces is negligible even when the crack is closed. The formula for G is exact in the absence of crack face friction. The mode mix, $\psi = \tan^{-1}(K_{II}/K_I)$, is only exact when there is no elastic mismatch. But deviations are small. For example, for a two layer system with $E_1/E_2 = 5$, the error in ψ given by (17) is less than 5° [15].

The solutions for a crack residing in layer 2 when specialized to the case of interest in Fig. 2, are given by:

$$K_I = \frac{P}{\sqrt{2Ah}} \cos \omega + \frac{M}{\sqrt{2}lh^3} \sin \omega \quad (18)$$

$$K_{II} = \frac{P}{\sqrt{2Ah}} \sin \omega - \frac{M}{\sqrt{2}lh^3} \cos \omega$$

Now, ω depends on the dimensionless parameter, $\lambda = (d/h) - 1$, and on the first Dundurs' elastic mismatch parameter, $\alpha_D = (\bar{E}_1 - \bar{E}_2)/(\bar{E}_1 + \bar{E}_2)$, as presented by [16]. The second Dundurs' parameter, β_D , has relative small numerical influence on the quantities of interest and will be regarded as zero. In addition, $A = \lambda + \Sigma$, where $\Sigma = (1 + \alpha_D)/(1 - \alpha_D)$. The position of the neutral bending axis of the bilayer above the plane of the delamination in (2) is given by $D = d - \Delta h$ with

$$A = \frac{\lambda^2 + 2\Sigma\lambda + \Sigma}{2(\lambda + \Sigma)} \quad (19)$$

while the moment of inertia of this bilayer is

$$I = \left(\Sigma \left[3(A - \lambda)^2 - 3(A - \lambda) + 1 \right] + 3A\lambda(A - \lambda) + \lambda^3 \right) / 3 \quad (20)$$

The energy release rate is

$$G = \frac{1}{2\bar{E}_2} \left(\frac{P^2}{Ah} + \frac{M^2}{lh^3} \right) \quad (21)$$

5. Solutions for equilibrium temperature distributions

The objectives of this section are to present energy release rates and mode mixities for delaminations in coatings subject to equilibrium temperature distributions. Several cases are explored.

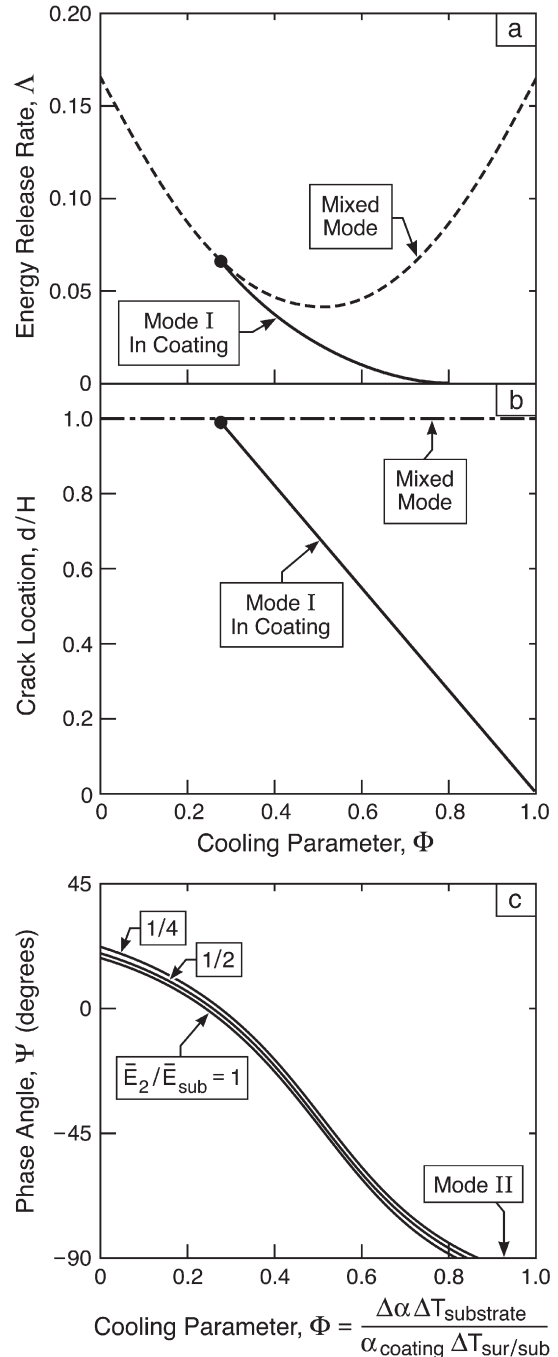


Fig. 6. (a) Energy release rate and (b) depth below the surface for a mode I delamination within a homogeneous coating and (c) the mode mix of the interface crack for three ratios of coating modulus. Also shown in (a) is the energy release rate for a delamination near the interface. The energy release rate parameter is, $A = \frac{G}{[(1+\nu_2)/(1-\nu_2)]E_2H(\alpha_{coating}\Delta T_{sur/sub})^2}$.

Case I is for a deep delamination in a homogeneous coating. As already noted, such delaminations can extend in mixed mode, so solutions for both G and ψ at $d/H=1$ are of interest. Case II considers shallower delaminations at $d/H < 1$. To address this case, initially we espouse the view that the delamination must be strictly mode I and present results for G with $\psi=0$, as a function of depth. The delaminations considered are either within a

homogeneous coating or internal to the dense layer, when present. Case III pertains to a deep delamination in a bilayer and provides solutions for G and ψ at $d/H=1$ as a function of the differences in thermo-elastic properties of the layers.

For a homogeneous coating, relevant to Cases I and II, the equilibrium temperature and stress distributions are linear through the coating

$$\sigma = \bar{\sigma} + \sigma_0(1 + 2\eta) \tag{22}$$

where $\bar{\sigma} = E_2\alpha_{\text{coating}}\Delta T_{\text{sur/sub}}(1/2 - \Phi)/(1 - \nu_2)$ and $\sigma_0 = [E_2\alpha_{\text{coating}}\Delta T_{\text{sur/sub}}/2(1 - \nu_2)]$. The quantities in (16) are

$$P = (\bar{\sigma} + \sigma_0)d - \sigma_0d^2/H \text{ and } M = \sigma_0d^3/(6H) \tag{23}$$

5.1. Case I

For a deep delamination ($d = H$), the steady-state energy release rate is given by:

$$G = \frac{H}{6E_2} (3\bar{\sigma}^2 + \sigma_0^2) \tag{24}$$

or

$$\frac{G}{[(1 + \nu_2)/(1 - \nu_2)]E_2H(\alpha_{\text{coating}}\Delta T_{\text{sur/sub}})^2} = \frac{(1 - 3\Phi + 3\Phi^2)}{6} \tag{25}$$

This result is plotted on Fig. 6a. The mode mix is

$$\begin{aligned} \psi &= \tan^{-1} \left(\frac{\sqrt{3} \bar{\sigma} \tan \omega - \sigma_0}{\sqrt{3} \bar{\sigma} + \sigma_0 \tan \omega} \right) \\ &= \tan^{-1} \left(\frac{\sqrt{3}(1 - 2\Phi)\tan \omega - 1}{\sqrt{3}(1 - 2\Phi) + \tan \omega} \right) \end{aligned} \tag{26}$$

When $\sqrt{3}(1 - 2\Phi) + \tan \omega < 0$, mode II pertains with $\psi = -\pi/2$. The dependence, $\omega(\alpha_D)$, is given in [17], where α_D is the Dundurs parameter measuring the elastic mismatch between the coating and the substrate. Note that ψ is weakly dependent on the mismatch (Fig. 6c).

5.2. Case II

For a shallower delamination, at $d < H$, subject to mode I conditions

$$\frac{M}{Pd} = \frac{1}{2\sqrt{3}} \tan \omega = 0.37 \tag{27}$$

such that

$$K_I = \frac{Pd^{-1/2}}{\sqrt{2\cos \omega}} = 1.15Pd^{-1/2} \text{ and } G = \frac{K_I^2}{E_2} = 1.325 \frac{P^2d}{E_2} \tag{28}$$

Thus, a mode I crack with $K_I > 0$ must have $P > 0$ and also, by (27), $M > 0$. Then, by (23), it follows that a mode I crack parallel to the surface with $d < H$ can only exist within the coating if $\sigma_0 > 0$ and $(\bar{\sigma} + \sigma_0) > 0$. These conditions highlight the necessity of a gradient of stress within the coating. Moreover, the gradient must be such that the stress at the surface of the coating is both tensile and greater than the stress at the interface.

The non-dimensional mode I energy release rate and crack location are:

$$\begin{aligned} \frac{G}{[(1 + \nu_2)/(1 - \nu_2)]E_2H(\alpha_{\text{coating}}\Delta T_{\text{sur/sub}})^2} &= 0.176(1 - \Phi)^3, \\ \frac{d}{H} &= 1.38(1 - \Phi) \end{aligned} \tag{29}$$

Note that necessary condition for mode I cracks to propagate within a homogeneous coating is $0.275 < \Phi < 1$. That is, upon initial cool-down ($\Phi = 0$), a mode I location does not exist within the coating. It only develops after the substrate has cooled sufficiently, when $\Phi \geq 0.275$ (Fig. 6b). At this instant, the energy release rate is a maximum and the delamination, if it forms, resides near the interface. Upon further cooling, the energy release decreases, and the location of the potential delamination moves closer to the surface.

The likelihood of forming a mode I delamination at specified depth, d/H , can be ascertained by eliminating the quantity Φ from (29) to give:

$$\frac{G}{[(1 + \nu_2)/(1 - \nu_2)]E_2H(\alpha_{\text{coating}}\Delta T_{\text{sur/sub}})^2} = 0.067(d/H)^3 \tag{30}$$

For shallow delaminations ($d/H \approx 0.1$), Eq. (30) indicates that the energy release rate is so small that their formation can be excluded under equilibrium conditions. Namely, transients are essential, as elaborated in Section 6.

When a dense layer is present and the delamination resides within that layer ($0 < d < h$), solutions are obtained in the same manner. Upon replacing the elastic properties with those for the dense layer, the outcome is

$$\begin{aligned} \frac{G}{[(1 + \nu_1)/(1 - \nu_1)]E_1H(\alpha_{\text{coating}}\Delta T_{\text{sur/sub}})^2} &= (0.176/c_1)(1 - \Phi)^3, \\ \frac{d}{H} &= (1.38/c_1)(1 - \Phi) \end{aligned} \tag{31}$$

where c_1 is given in (3).

5.3. Case III

When a dense layer is present and the crack lies below that layer ($h < d < H$), the expressions based on (18)–(21) are more complicated, but they can still be obtained in

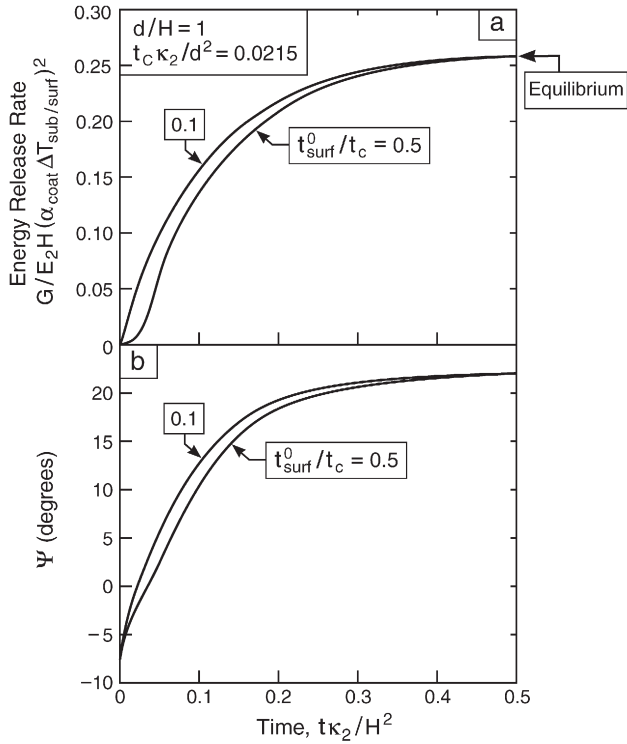


Fig. 7. Transient energy release rate and mode mix of a crack near the interface (depth $d/H=1$) in a homogeneous coating for two surface cool down times plotted over the time scale required to equilibrate the temperature distribution across the entire coating (long compared to t_c).

closed form (Appendix B). The dimensionless stress intensity factors depend linearly on Φ , and it is straightforward to find Φ corresponding to a specified d/H . The dimensionless forms are:

$$\frac{G}{E_2 H (\alpha_{\text{coating}} \Delta T_{\text{surf/sub}})^2} = f\left(\frac{E_1}{E_2}, \frac{k_1}{k_2}, \frac{h}{H}, \nu_1, \nu_2, \Phi\right), \quad (32)$$

$$\frac{d}{H} = g\left(\frac{E_1}{E_2}, \frac{k_1}{k_2}, \frac{h}{H}, \nu_1, \nu_2, \Phi\right)$$

The functions f and g are presented in Appendix B. A program has been written that allows these functions to be plotted for any defined parameters. Examples will be presented below.

6. Solutions for temperature transients

In this section, assessment is made of the possibility that the susceptibility to delamination might be more likely during the transient, prior to attaining temperature equilibrium. This possibility is examined separately for deep and shallow delaminations. The preceding Case II assessment has already indicated that shallow delaminations are unlikely under equilibrium conditions. Their incidence during the transient is analyzed by combining (9), (16) and (17) [14,18] to reveal that

at every depth d the crack experiences mode I at a specific time given by

$$t_c = 0.0215 d^2 / \kappa \quad (33)$$

with associated intensity factor and energy release rate:

$$K_I = 0.190 \frac{E \alpha \Delta T_{\text{surf/sub}} \sqrt{d}}{(1-\nu) G}, \quad (34)$$

$$\frac{G}{[(1+\nu_2)/(1-\nu_2)] E H (\alpha_{\text{coating}} \Delta T_{\text{surf/sub}})^2} = 0.036 d / H$$

Here $\Delta T_{\text{surf/sub}} = T_{\text{surface}}^i - T_{\text{surface}}^f$ and E takes on the value relevant to the material incorporating the delamination. That is, a crack at any depth will experience mode I conditions at one instant during cool-down.

For shallow delaminations, this energy release rate is much larger than the equilibrium value (30): affirming that such delaminations are more probable during the transient. This result is directly applicable to delaminations within the dense layer provided that the rate of cool down is sufficiently rapid that the temperature at the surface reaches T_{surface}^f at times short compared to t_c , and the substrate must have only modest influence on the temperature at that instant.

For deep delaminations, near the interface, both G and ψ are pertinent. Results derived using the temperatures and stresses

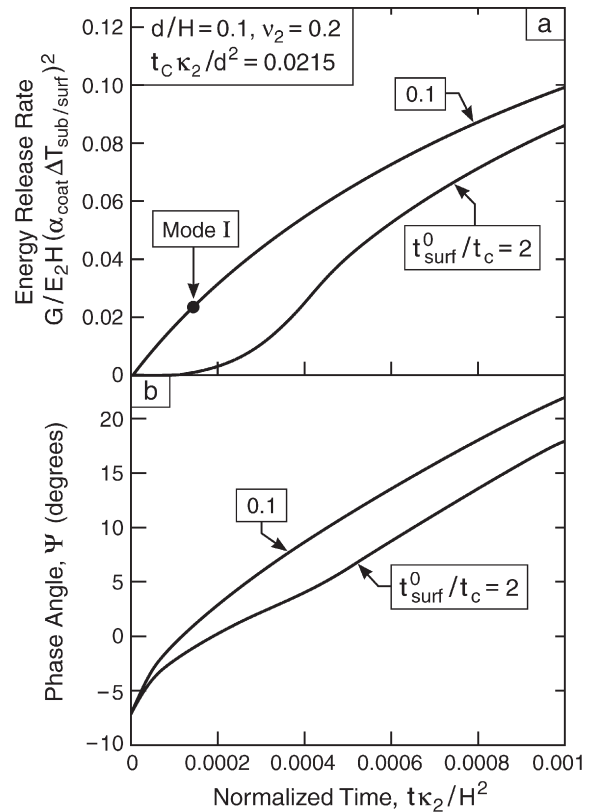


Fig. 8. Transient energy release rate and mode mix of a shallow ($d/H=0.1$) crack in a coating with dense layer thickness, $h/H=0.5$. Curves are plotted for two surface cool down times over the time scale comparable to t_c defined in (33). For short cool-down times the mode I energy release rate is accurately predicted by (34) using the properties of the dense layer.

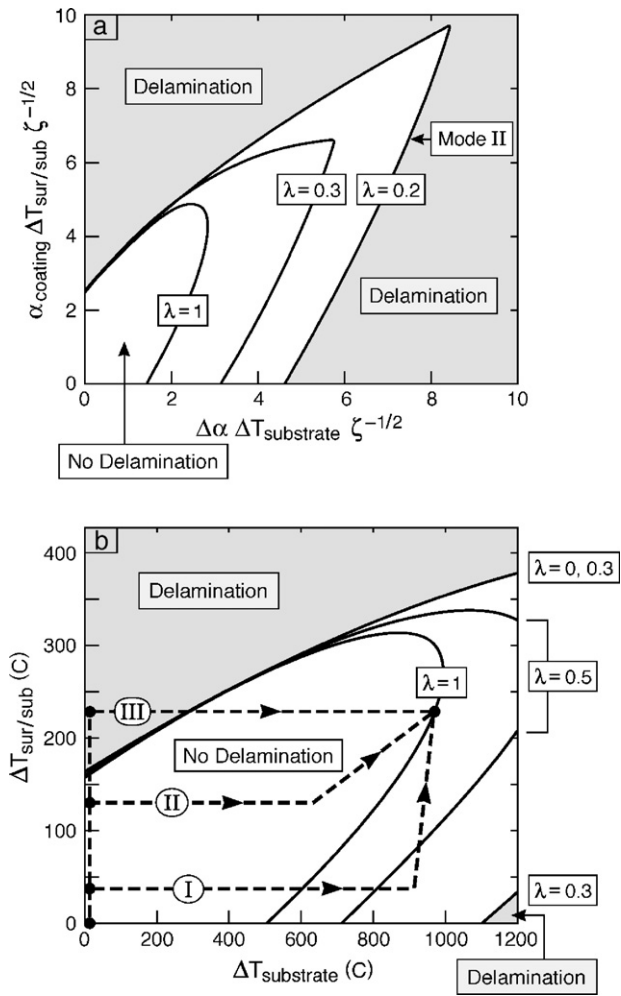


Fig. 9. Delamination maps for homogeneous coatings determined for equilibrium cool-down histories. (a) Dimensionless boundaries. (b) Boundaries for a 1 mm thick homogeneous APS–TBC (properties in Table 1) on a superalloy substrate. Deep delamination cannot take place during cool-down provided that the combination of temperature drops ($\Delta T_{\text{substrate}}$, $\Delta T_{\text{sur/sub}}$) does not cross any of the boundaries at the relevant mode mix. Three cool-down trajectories illustrate: (I) late-stage delamination ($\lambda=0.5$), (II) delamination-safe, (III) early-stage delamination.

from Section 3 for a homogeneous coating are plotted on Fig. 7. The energy release rates increase systematically with time and asymptote to the equilibrium limit [(25) with $\Phi=0$] at $t\kappa_2/H^2 \approx 1/2$ (see also the result in Fig. 6a). At $t < t_c$ the crack experiences relatively small negative ψ and then transitions to positive ψ as the energy release rate increases. An accurate estimate of the small negative value at the earliest times can be obtained by assuming a very thin thermally stressed layer equivalent to a force/length, P , acting at the surface. Then, by (16), $M=Pd/2$, and by (17),

$$K_I = \frac{Pd^{-1/2}}{\sqrt{2}} \left[\cos\omega + \sqrt{3}\sin\omega \right]$$

$$K_{II} = \frac{Pd^{-1/2}}{\sqrt{2}} \left[\sin\omega - \sqrt{3}\cos\omega \right]$$

with $\omega = 52.1^\circ$, $\psi = \tan^{-1}(K_{II}/K_I) = -7.9^\circ$. Thus, a delamination at any depth below the surface experiences an initial period having small negative ψ . The effect of a dense layer ($h/H=0.5$) is shown in Fig. 8 for a shallow delamination ($h/H=0.1$). As expected from previous examples, the basic solution, (33) and (34), (with $E=E_1$ and $\kappa=\kappa_1$) provides an excellent approximation for the mode I loading of the shallow crack as long as (t^0_{surface}/t_c) is sufficiently small.

7. Mechanism maps for deep delaminations

Homogeneous coating. By imposing $G=\Gamma_C^{(i)}$ and using (1) and (25), the following equation characterizes delamination boundaries for $d=H$:

$$Y^2 - 3YX + 3X^2 = 6[1 + \tan^2((1-\lambda)\psi)] \tag{35}$$

where the dimensionless cool-down coordinates are

$$X = \Delta\alpha\Delta T_{\text{substrate}}\zeta^{-1/2}, Y = \alpha_{\text{coating}}\Delta T_{\text{sur/sub}}\zeta^{-1/2} \tag{36}$$

with

$$\zeta = \left[\frac{(1-\nu_2)\Gamma_{IC}^{(i)}}{(1+\nu_2)E_2H} \right]$$

The mode mix, ψ , can be expressed in terms of $\Phi=X/Y$ by using (26). Boundaries from (35) are plotted in Fig. 9a for several λ , ranging from the mode-independent toughness, $\lambda=1$, to strong mode-dependence, $\lambda=0.2$. The map is re-plotted in dimensional form (Fig. 9b) for a 1 mm thick APS–TBC having the properties listed in Table 1, with $\lambda \geq 0.25$. These maps specify delamination conditions for any equilibrium-cooling scenario. To ascertain the actual incidence of delamination, *cooling trajectories* must be superposed. If a trajectory enters one of the shaded domains, a delamination is predicted. To illustrate the application of the maps, three possible trajectories

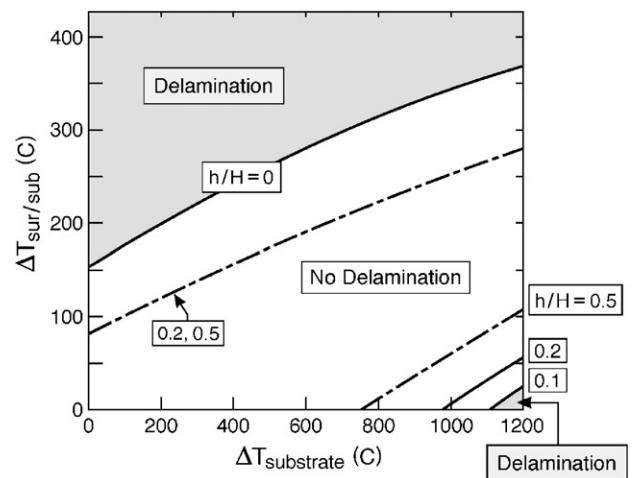


Fig. 10. A map for deep delamination in an APS–TBC on a superalloy substrate with CMAS infiltration to depth, h/H . The mixed mode toughness parameter is, $\lambda=0.25$.

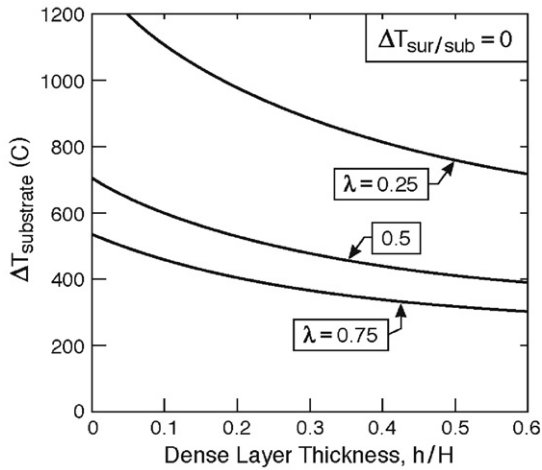


Fig. 11. The relationship between substrate cool-down temperature and the conditions for delamination in accordance with trajectory I on Fig. 9, plotted as a function of the dense layer thickness for several values of the mixed mode toughness parameter.

have been plotted on Fig. 9b, all having the same initial condition: namely a substrate at temperature, $T_{\text{sub}}^i = 900$ °C and a TBC surface temperature, $T_{\text{surf}}^i = 1130$ °C. With the premise that (for this TBC) the mixity coefficient is, $\lambda = 0.5$, only trajectory II is fail-safe. Namely, for this trajectory, the combination of the instantaneous values of $\Delta T_{\text{sur/sub}}$ and $\Delta T_{\text{substrate}}$ always remains entirely within the boundaries. The other trajectories allow delamination: albeit at two different stages of cool-down. Trajectory III involves initial rapid cooling of the surface with substrate temperature unchanged ($\Delta T_{\text{substrate}} = 0$) until the coating and substrate temperatures equalize, followed by gradual cool-down. This trajectory crosses a boundary during initial cooling, causing instantaneous

delamination. Note that this boundary is only weakly dependent on λ (because the delamination is predominantly mode I: see Fig. 6c for $\Phi = 0$). Trajectory I reveals that, even if early stage delamination is avoided, by retaining $\Delta T_{\text{sur/sub}} \approx 0$, it can still occur during slow cooling, should the trajectory cross the right-side contour (at the relevant λ). This boundary exists because the average tension in the coating decreases and becomes compressive as $\Delta T_{\text{substrate}}$ increases. It depends strongly on λ , since it is associated with a mode II crack. One additional note: for the same initial substrate temperature $T_{\text{sub}}^i = 900$ °C, if the initial temperature difference across the TBC satisfied, $\Delta T_{\text{sur/sub}} \geq 350$ °C, such that the end-point resided in the top right of the upper shaded domain, the TBC would delaminate regardless of the cooling trajectory. Namely, for this case, the ambient temperature energy release rate exceeds the TBC toughness at the pertinent mode mix. This situation is examined elsewhere in more detail [10].

For coatings with a dense layer, given the large number of parameters, delamination contours are presented only in dimensional form. The system selected is that for a 1 mm thick APS–TBC on an engine shroud in which the dense layer has arisen because CMAS has penetrated to a depth, $h/H = 0.5$ [10]. Results are computed using the formulas for two-layer systems given in Appendix B and the properties from Table 1, with $\lambda = 0.25$ (Fig. 10). The contour for the homogenous TBC ($h/H = 0$) is included in the figure. Evidently, the dense layer increases the susceptibility to delamination by closing down the delamination-free domain on the mechanism map. The maximum levels are roughly halved for infiltration to depth, $h/H \geq 0.2$. The lowering of the $\Delta T_{\text{sur/sub}}$ intercept saturates at larger h/H , suggesting that the maximum degradation upon rapid surface cooling is approached at a penetration depth of about 20% the coating thickness. For other cooling trajectories, the incidence of delaminations varies in a more systematic manner, as illustrated by results for trajectories of type I, plotted on Fig. 11. For such

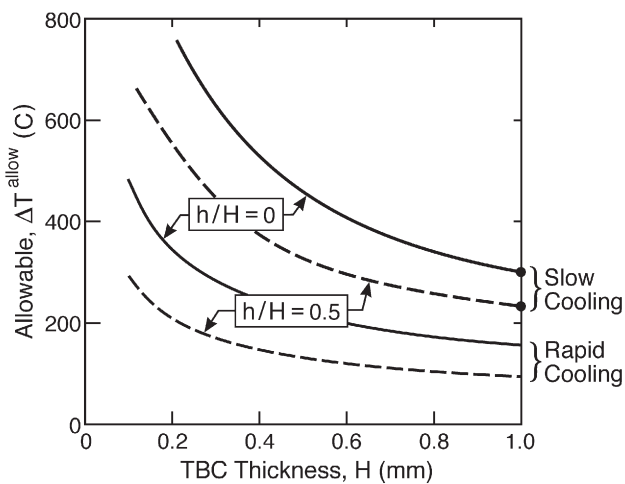


Fig. 12. Plots of the allowable temperature difference as a function of the TBC thickness, H , for deep delaminations ($d/H = 1$). The two lower plots are for a rapid initial cooling trajectory (type III on Fig. 9), with and without a dense layer. The upper two are the corresponding plots for a slow-cooling trajectory type I.

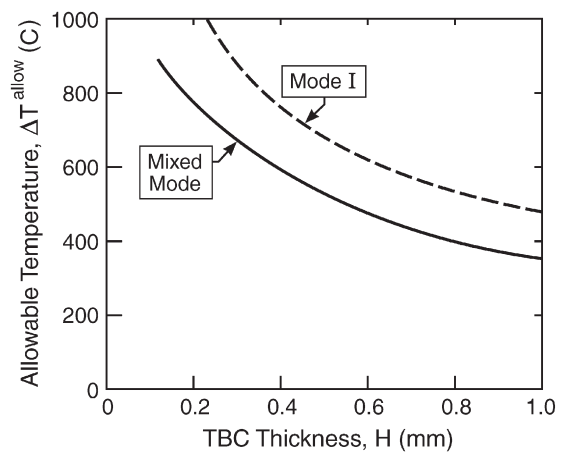


Fig. 13. Plots of the allowable temperature difference as a function of the TBC thickness, H , for shallow delaminations ($d/H = 0.1$). The uppermost is for a situation requiring that the delamination be strictly mode I. The lower allows for the possibility that the delamination can extend parallel to the surface with limited mode II ($\psi \leq 5^\circ$).

cooling trajectories, the influence of a dense layer thickness is strongly affected by the mode mixity parameter, λ .

8. Illustration of temperature allowables

The preceding results can be converted into temperature allowables, ΔT^{allow} , for any thermal scenario and any TBC, with or without a dense layer. In principle, these ΔT^{allow} could be compared with engine experience. In practice, the thermal scenarios in engines are not sufficiently well-defined to enable a definitive assessment. Instead, the trends are discussed with reference to the thermal situation applicable to airfoils and shrouds. The allowables concept is illustrated for deep delaminations ($d/H=1$), exemplified by those at level (i) in the shroud (Fig. 1b). Two cooling trajectories are examined; One characterized by a rapid drop in surface temperature, represented by trajectory III on Fig. 9b; the other by slow cooling along trajectory I. The allowables for these trajectories are plotted on Fig. 12, with and without a dense layer. For thin (0.1 mm thick) coatings of the type used on airfoils, the allowables are consistent with engine experience. Namely, the surface temperature can drop suddenly by as much as, ($\Delta T^{\text{allow}} \approx 500$ °C, without causing delamination. This allowable is significantly in excess of the temperature difference ($T_s - T_o$) imposed across the TBC in actual engines. With a dense layer caused by CMAS penetration, the allowable is diminished, $\Delta T^{\text{allow}} \approx 300$ °C, but still comparable to $T_s - T_o$ in hot regions of the airfoil, where the CMAS (when present) has melted ($T_{\text{CMAS}}^{\text{melt}} = 1220$ °C) [10]. For a thick (1 mm) coating, of the type used on shrouds, the sustainable surface temperature drop is only, $\Delta T^{\text{allow}} = 160$ °C, even without a dense layer. The corresponding allowable for gradual cool-down (trajectory I in Fig. 9b) is $\Delta T^{\text{allow}} \approx 350$ °C: similar to the actual temperature difference experienced by shrouds [10]. Since shrouds without CMAS survive, the inference is that these components do not normally experience rapid surface cooling. When CMAS penetrates to $h/H > 0.2$, the trajectory I allowable reduces to $\Delta T^{\text{allow}} \approx 220$ °C, consistent with the occurrence of delaminations in penetrated regions of the shroud [10].

The corresponding results for shallow delaminations within the dense layer, obtained from analysis of the transient, are plotted on Fig. 13. One plot refers to circumstances requiring strictly mode I propagation. The other allows the possibility that they can extend parallel to the surface with a small component of mode II, not exceeding, $\psi = 5^\circ$. In thin TBCs (of the type shown in Fig. 1a), large temperature allowables for avoidance of shallow delaminations are implied: 1200 °C for mode I and 800 °C for limited mixed mode. The possibility that such severe transients can happen is presently unknown. Evidently, much remains to be discovered about temperature gradients in actual engines before the present mechanics solutions and mechanism maps can be adequately validated.

9. Conclusion

The mechanics of delaminations in coatings that experience thermal gradients have been presented. Results are provided

for homogeneous coatings and for bilayers with a dense outer layer, typical of those that form as a consequence either of sintering or of CMAS penetration. Detailed solutions have been generated for delaminations at two locations in the coating, motivated by observations made on components removed from hot sections of aeroengines. One set refers to deep delaminations, just above the substrate, for which equilibrium temperatures at the end of the transient are relevant. The other applies to shallow delaminations within the dense outer layer (when present), for which the transient cooling stage is most critical.

A detailed analysis has been presented for deep delaminations by ascertaining the equilibrium energy release rate and mode mixity, and incorporating a mode dependent criterion. The outcome is a set of delamination maps, illustrated for coatings with and without a dense layer. The maps are implemented by superposing cooling trajectories. Such implementations reveal that, even for the same initial temperature distributions during operation, the incidence of delamination is sensitive to the cooling trajectory.

The most severe cooling trajectories have been identified. These have been used to develop temperature allowables and a cursory comparison made with engine experience. But because the temperatures experienced by the coatings in the engine are not well-specified the correlations are inconclusive. To provide a higher fidelity validation of the mechanics, future experimental assessments will be conducted with defined temperature gradients and a range of cooling scenarios.

Appendix A. Transient temperature distribution

The equilibrium temperature distribution at any instant, ($T_{\text{equil}}(\eta, t)$), introduced in (12) satisfies the interface condition (11), together with the steady-state equation, $T_{\text{equil},yy} = 0$. Thus, upon substitution of the representation (12) into (10), one finds that δT must satisfy the inhomogeneous diffusion equation

$$\begin{aligned} \delta T_{,yy} - \kappa^{-1} \delta T_{,t} \\ = \kappa^{-1} \left(A(\eta) \frac{dT_{\text{surface}}}{dt} + B(\eta) \frac{dT_{\text{substrate}}}{dt} \right) \end{aligned} \quad (\text{A.1})$$

As in (10), κ takes on the value κ_1 or κ_2 in the respective layers; δT must also satisfy the interface condition (11). The boundary conditions and initial condition on δT are homogeneous because T_{equil} satisfies the boundary conditions at $\eta = 0$ and $\eta = -1$ at all times and it coincides with the initial steady-state distribution at $t = 0$; thus,

$$\delta T(0, t) = \delta T(-H, t) = \delta T(y, 0) = 0$$

This completes the specification of the problem for δT .

The set of eigenfunctions, $\{f_n(\eta)\}$, used in the expansion of δT on $-1 \leq \eta \leq 0$ are constructed such that each one satisfies the interface condition (11). With λ_n as the eigenvalue, $f_n(\eta)$ is required to satisfy

$$p d^2 f_n / d^2 \eta + \lambda_n f_n = 0 \quad (\text{A.2})$$

with $p=1$, $-h/H < \eta \leq 0$ and $p=k_1/k_2$, $-1 < \eta \leq -h/H$. The boundary conditions are $f_n(0)=0$ and $f_n(-1)=0$. Continuity of f_n at $\eta=-h/H$ is required together with

$$\lim_{\varepsilon \rightarrow 0} k_1 f'_n(-h/H + \varepsilon) = k_2 f'_n(-h/H - \varepsilon).$$

The eigenvalue equation resulting from the above is

$$\sqrt{\frac{k_1}{k_2}} \tan \left[\sqrt{\lambda_n} \left(1 - \frac{h}{H} \right) \right] + \tan \left[\sqrt{\frac{k_2 \lambda_n}{k_1}} \frac{h}{H} \right] = 0 \quad (n = 1, \infty) \quad (\text{A.3})$$

and the associated eigenfunctions are

$$\begin{aligned} f_n &= -\mu_n \sin \left(\sqrt{k_2 \lambda_n / k_1} \eta \right), \quad -h/H < \eta \leq 1 \\ &= \sin(\sqrt{\lambda_n} (1 + \eta)), \quad -1 \leq \eta < -h/H \end{aligned} \quad (\text{A.4})$$

with $\mu_n = \sin(\sqrt{\lambda_n} (1 - h/H)) / \sin(\sqrt{k_2 \lambda_n / k_1} h/H)$. The orthogonality relations are: $\int_{-1}^0 f_n f_m d\eta = 0$ for $m \neq n$.

The solution for the departure from equilibrium is written as

$$\delta T(\eta, \tau) = \sum_{n=1}^M a_n(\tau) f_n(\eta) \quad (\text{A.5})$$

with dimensionless time variable, $\tau = \kappa_2 t / H^2$. Substitution of (A.5) into (A.1) and use of the standard Galerkin procedure leads to a set of M coupled first order, ordinary differential equations for the a_n . The set becomes decoupled if the heat capacity, ρ , is the same in each layer. The relation among diffusivity, conductivity and heat capacity is $k = \rho \kappa$, and, thus, $k_1/k_2 = (\rho_1/\rho_2)(\kappa_1/\kappa_2)$. Because the volume fraction of CMAS in the infiltrated layer of the TBC is relatively small, it is expected to have only slight effect on heat capacity. Thus, to simplify the analysis, we have taken $\rho_1 = \rho_2$ and, therefore, $(k_1/k_2) = (\kappa_1/\kappa_2)$. In this case, the general solution is found to be

$$a_n(\tau) = -\frac{e^{-\lambda_n \tau}}{C_n} \left\{ A_n \int_0^\tau e^{\lambda_n \zeta} \frac{dT_{\text{surface}}(\zeta)}{d\tau} d\zeta + B_n \int_0^\tau e^{\lambda_n \zeta} \frac{dT_{\text{substrate}}(\zeta)}{d\tau} d\zeta \right\} \quad (\text{A.6})$$

for $n=1, M$ where

$$\begin{aligned} A_n &= \int_{-1}^0 A(\eta) f_n(\eta) d\eta, B_n = \int_{-1}^0 B(\eta) f_n(\eta) d\eta, \\ C_n &= \int_{-1}^0 f_n^2(\eta) d\eta, \end{aligned}$$

and $d(\)/d\tau = (H^2/\kappa_2) d(\)/dt$.

Numerical solutions presented in the paper were generated with $M=50$. Repetition of computations at selected values of the input parameters showed that most results were given to an accuracy of a fraction of a percent with $M=10$, and in all cases checked the choice $M=50$ was more than sufficient for generating the temperature distribution with high accuracy.

Appendix B. Steady-state delamination in the coating below the dense layer

Based on the stress distribution (5), the integrations in (16) give

$$\begin{aligned} \frac{P}{HE_2 \alpha_{\text{coating}} \Delta T_{\text{sur/sub}}} &= p_A + p_B \Phi, \\ \frac{M}{H^2 E_2 \alpha_{\text{coating}} \Delta T_{\text{sur/sub}}} &= m_A + m_B \Phi \end{aligned} \quad (\text{B.1})$$

where

$$\begin{aligned} p_A &= \frac{E_1}{E_2(1-\nu_1)} \left(\frac{h}{H} - \frac{1}{2} c_1 \left(\frac{h}{H} \right)^2 \right) + \frac{c_2}{(1-\nu_2)} \left(\frac{d}{H} - \frac{h}{H} - \frac{1}{2} \left(\left(\frac{d}{H} \right)^2 - \left(\frac{h}{H} \right)^2 \right) \right) \\ p_B &= -\frac{E_1}{E_2(1-\nu_1)} \frac{h}{H} + \frac{1}{(1-\nu_2)} \left(-\frac{d}{H} + \frac{h}{H} \right) \\ m_A &= q p_A + \frac{E_1}{E_2(1-\nu_1)} \left(-\frac{1}{2} \left(\frac{h}{H} \right)^2 + \frac{1}{3} c_1 \left(\frac{h}{H} \right)^3 \right) + \frac{c_2}{(1-\nu_2)} \left(-\frac{1}{2} \left(\left(\frac{d}{H} \right)^2 - \left(\frac{h}{H} \right)^2 \right) + \frac{1}{3} \left(\left(\frac{d}{H} \right)^3 - \left(\frac{h}{H} \right)^3 \right) \right) \\ m_B &= q p_B + \frac{E_1}{2E_2(1-\nu_1)} \left(\frac{h}{H} \right)^2 + \frac{1}{2(1-\nu_2)} \left(\left(\frac{d}{H} \right)^2 - \left(\frac{h}{H} \right)^2 \right) \\ q &= (1 + \lambda - \Delta) h/H \end{aligned}$$

These expressions allow for direct computation of K_1 and K_2 using (18). Noting from (B.1) that the stress intensity factors are linear in Φ , one can readily determine the value of Φ corresponding to $K_2 = 0$ for any given crack depth.

References

- [1] R.A. Miller, J. Am. Ceram. Soc. 67 (1984) 517.
- [2] T.E. Strangman, Thin Solid Films 127 (1985) 93.
- [3] P.K. Wright, Mater. Sci. Eng., A Struct. Mater.: Prop. Microstruct. Process. 245 (1998) 191.
- [4] A.G. Evans, D.R. Mumm, J.W. Hutchinson, G.H. Meier, F.S. Pettit, Prog. Mater. Sci. 46 (2001) 505.
- [5] D.R. Clarke, C.G. Levi, Ann. Rev. Mater. Res. 33 (2003) 383.
- [6] N. Padture, M. Gell, E. Jordan, Science 296 (2002) 280.
- [7] M.J. Stiger, N.M. Yanar, M.G. Toppings, F.S. Pettit, G.H. Meier, Z. Met. kd. 90 (1999) 1069.
- [8] M.P. Borom, C.A. Johnson, L.A. Peluso, Surf. Coat. Technol. 86–87 (1996) 116.
- [9] C. Mercer, S. Faulhaber, A.G. Evans, R. Darolia, Acta Mater. 53 (2005) 1029.
- [10] Faulhaber, S., Kraemer, S., Levi, C., Clarke, D.R., Hutchinson, J.W., and Evans, A. G., in press.
- [11] G.R. Dickson, C. Petorak, K. Bowman, R.W. Trice, J. Am. Ceram. Soc. 88 (2005) 2202.
- [12] D. Zhu, R.A. Miller, International Conference on Engineering Ceramics and Structures; American Ceramic Society, Cocoa Beach, Florida, January 23–28, 2000.
- [13] T. Xu, S. Faulhaber, C. Mercer, M. Maloney, A. Evans, Acta Mater. 52 (2004) 1439.
- [14] J.W. Hutchinson, Z. Suo, Adv. Appl. Mech. 29 (1992) 63.
- [15] J.W. Hutchinson, M.E. Mear, J.R. Rice, J. Appl. Mech. 54 (1987) 828.
- [16] Z. Suo, J.W. Hutchinson, Int. J. Solids Struct. 25 (1989) 1337.
- [17] Z. Suo, J.W. Hutchinson, Int. J. Fract. 43 (1990) 1.
- [18] L.G. Zhao, T.J. Lu, N.A. Fleck, J. Mech. Phys. Solids 48 (2000) 867.
- [19] M. Watanabe, C. Mercer, C.G. Levi, A.G. Evans, Acta Mater. 52 (2004) 1479.
- [20] J.B. Wachtman, Mechanical Properties of Ceramics, Wiley, 1996.
- [21] S.Q. Guo, D.R. Mumm, A.M. Karlsson, Y. Kagawa, Scripta Materialia 53 (2005) 1043.
- [22] S. Lampenscherf, Private Communication, Siemens AG, 2006.
- [23] C.A. Johnson, J.A. Ruud, R. Bruce, D. Wortman, Surf. Coat. Technol. 108/109 (1998) 80.
- [24] A. Rabiei, A.G. Evans, Acta Mater. 48 (2000) 3963.